Earth Sciences
2017; 6(5): 88-96
http://www.sciencepublishinggroup.com/j/earth
doi: 10.11648/j.earth.20170605.15
ISSN: 2328-5974 (Print); ISSN: 2328-5982 (Online)

Curie Point Depth from Spectral Analysis of Magnetic Data in the Southeast Tibet

Kai Yang[1, 2], Junhui Xing[1, 2, 3, *], Wei Gong[1, 2], Chaoyang Li[1, 2], Xiaoyang Wu[1, 2]

[1]The Key Lab of Submarine Geosciences and Prospecting Techniques, Ministry of Education, Qingdao, China

[2]Evaluation and Detection Technology Laboratory of Marine Mineral Resources, Qingdao National Laboratory for Marine Science and Technology, Qingdao, China

[3]College of Marine Geosciences, Ocean University of China, Qingdao, China

Email address:

junhuixing@ouc.edu.cn (Junhui Xing)

[*]Corresponding author

To cite this article:

Kai Yang, Junhui Xing, Wei Gong, Chaoyang Li, Xiaoyang Wu. Curie Point Depth from Spectral Analysis of Magnetic Data in the Southeast Tibet. *Earth Sciences*. Vol. 6, No. 5, 2017, pp. 88-96. doi: 10.11648/j.earth.20170605.15

Received: June 27, 2017; **Accepted**: July 11, 2017; **Published**: September 18, 2017

Abstract: The satellite magnetic anomalies are used to calculate the Curie point depth of the Southeast Tibet by spectral analysis method in the study. The relationship between the Curie point depth and the regional faults or heat flow will be discussed. The results show that the Curie point depth of the study area ranges from 15 km to 36 km and the average depth is 26.3 km. The Curie point depth is cluster-like on the north of the Ailaoshan-Red River Fault, while it is strip-like distribution on the north side. The Curie point depth in the Xiaojiang Fault zone, the Xiaojinhe Fault zone, the Dien Bien Phu Fault zone and the Gaoligong Fault zone are shallow. It could be related to their strong frictional heat induced by these faults. The Curie point depth in the middle Sukhothai Block is shallow, which it is not only related to the Phayao Fault, the Mae Chan Fault and the Nam Ma Fault, but also to the subduction of the Palaeo-Tethys into the Indochina Block. There is a negative but nonlinearly correlation between the heat flow and the Curie point depth in this study area. The areas of low heat flow value correspond to the areas of deep Curie point depth. However, both the high and low heat flow values can be found in the areas of shallow Curie point depth. The possible reason is thought to be related to the low thermal conductivity of the rock.

Keywords: Magnetic Anomalies, Spectral Analysis, Curie Point Depth, Heat Flow, The Southeast Tibet

1. Introduction

The Curie point depth (CPD, also called Curie isothermal surface) refers to the thermal surface for the ferromagnetic crustal rocks transforming to paramagnetic rocks when the temperature reach the Curie point [1]. It is the bottom of the magnetic layer in the lithosphere. The CPD reflects the thermal state of the lithosphere rather than the geologic tectonic surface, so that it is not appropriate to be measured by the geological markers.

As a crustal thermal boundary, the CPD reflects the thermodynamic structure of the crust. Many scientists demonstrated the CPD distributed characteristics of different areas due to its meaningful reflection of tectonic settings, geothermal distribution and volcanic activity. Tanaka et al. [2] calculated the CPD in East Asia and found that the CPD distribution varied greatly according to the geological context. The CPD are shallower than 10 km at volcanic and geothermal areas, about 15-25 km at island arcs and ridges and deeper than about 20 km at plateaus, respectively. In the west part of Anatolian, Turkey, the study on the CPD showed a geothermal anomaly area, which the length is 350 km and the width is 100 km. It is considered that the asthenosphere upwelling caused by the lithosphere extension formed the anomaly area [3]. The CPD in Sinai Peninsula, Egypt showed that seismicity generally occurred in shallow CPD locations and the Suez Bay is developed about the prospect of geothermal resources [4]. Kasidi and Nur [5] studied the CPD distribution in northeast part of Nigeria and found that the CPD is negatively correlated with the heat flow. The CPD ranged from 30-40 km in the central Brazil, which induced that three magnetic layers were existed in this region [6]. Comparison the CPD in Taiwan with

the measured heat flow, the results showed that the CPD is negatively correlated with the measured heat flow with correlation coefficient 0.62 [7].

As a lateral collision zone and material escape zone induced by the Indian and the Eurasian plate, the southeast Tibet consists of various blocks and faults, which is developed in different stages. The complex geological structure has been attracting the attention of numerous scholars. Part of them tried to reveal the tectonic structure and fault activity characteristics based on the study of the CPD. According to the calculation of the CPD in Kang-Dian continental paleo-rift zone using aeromagnetic data, the authors concluded that the CPD in rigid block is deep, whereas the edge of the block is shallow [8]. Using satellite magnetic data, Gao et al. [9] studied the CPD in southeast Tibet in China. They found that the CPD uplift zones near large deep faults correspond to the faults and the distribution of the magnetic anomaly reflects the escape flow from east Tibet.

The study area is in the intersection of multiple blocks as well as the complexity of the geological structure. The deep and comprehensive discussions about the CPD distributed characteristics and the influence of the geological structure on the CPD distribution is rare. In this paper, the CPD of the study area is calculated by using satellite magnetic anomaly data with spectral analysis method. And then, the causes of the distribution of the CPD from the perspective of geological structure are discussed. Additionally, the relationship between the CPD and the heat flow is also discussed.

2. Geological Settings

The study area is located in the southeast Tibet, which is composed by eight blocks (Figure 1): the Northwest Sichuan Block, the Central Yunnan Block, the Eastern Yunnan Block, the Sibumasu Block, the Sukhothai Block, the Lanping-Simao Block，the Indochina Block and the Song Da Block. Major faults (e.g., the Ailaoshan-Red River Fault (RRF), the Xiaojinhe Fault (XJHF), the Xiaojiang Fault (XJF), the Gaoligong Fault (GLGF) and the Dien Bien Phu Fault (DBPF)) can be identified in southeast Tibet [9-10]. The RRF is an important transition zone among the blocks in study area. Its formation is caused by the collision between Indian and Eurasian plate. The tectonic movement of the fault is left lateral strike slip ductile shearing at early stage, while it is the right lateral strike slip at late stage. The average slip rate of the RRF since Quaternary is about 4-5 mm/y [11]. The RRF is a large deep fault in the Himalayan orogeny. The fault was formed during the end of Paleozoic and Mesozoic caused by the collision between the Gondwana and Eurasian Plate. The Yangtze Block is located in the north of the RRF, while the adjoining region between the East Tethys tectonic domain and the western Pacific tectonic domain is located in the south of the RRF [12-16]. The Chuan-Dian rhombic block (CDRB) located in the southwest Yangtze plate consists of the Northwest Sichuan Block and the Central Yunnan Block. The western boundary of CDRB is the RRF while the eastern boundary is the XJF.

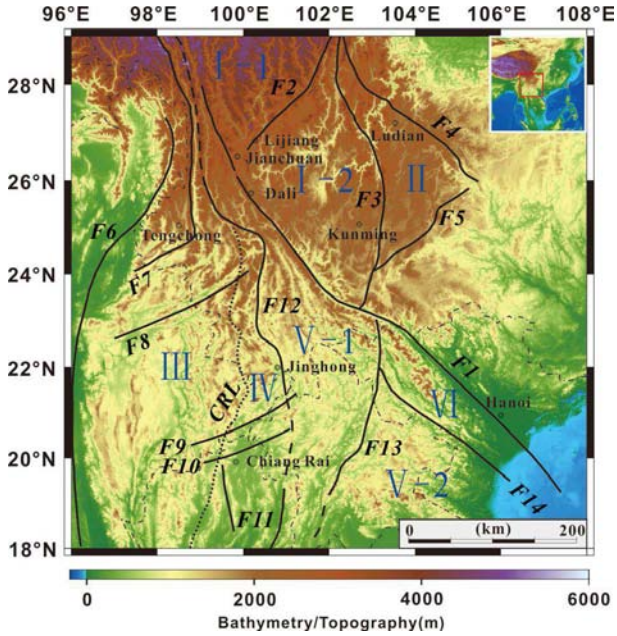

Figure 1. *Topography and geological subdivisions of the Southeast Tibet. I-1: Northwest Sichuan Block; I-2: Central Yunnan Block; II: Eastern Yunnan Block; III: Sibumasu Block; IV: Sukhothai Block; V-1:Lanping-Simao Block; V-2:Indochina Block; VI: Song Da Block; F1:Ailaoshan-Red River Fault; F2:Xiaojinhe Fault; F3:Xiaojiang Fault; F4:Kangding–Yiliang–Shuicheng Fault; F5:Mile–Shizong–Shuicheng Fault; F6:Sagaing Fault; F7:Gaoligong Fault; F8:Nanting Fault; F9:Nam Ma Fault; F10:Mae Chan Fault; F11:Phayao Fault; F12:Lancangjiang Fault; F13:Dien Bien Phu Fault; F14:Song Ma Suture; CRL: Chiang Rai Line. In the study area, the blocks are mainly bounded by faults. The Sukhothai Block is bounded by CRL and F12, and the Sibumasu Block is bounded by F6, F12 and CRL. (Modified after Gao et al.[9]; Metcalfe [10]; Tun et al.[17]; Noisagool et al. [18]).*

The crustal material in the southeast Tibet moves eastward due to the collision between the Indian plate and the Eurasian plate. Previous studies show a southward displacement of the CDRB during the last 12 m. y [19-22]. Lv et al. [23] suggested the relatively stable South China block blocked the eastward movement of CDRB, and the direction of the CDRB motion changed from east to south along the XJF zone. The XJF zone as the eastern boundary of the CDRB is a left lateral strike slip active fault with intense internal heat action and high frequent earthquakes [24]. The major geological structures in the south of the RRF are the GLGF zone, the Sukhothai Block and the DBPF zone. The GLGF zone is derived from the northward subduction of the Indian plate beneath the Eurasian plate. The Tengchong volcano area is characterized as strong shear deformation and frequent magmatic activity. Therefore, the Tengchong volcano area is one of the most abundant geothermal resources in China. The Sukhothai Arc is located in the Sukhothai Block. Its formation can be traced back to the subduction of Paleo-Tethys to the Indochina Block in the Latest Carboniferous or very Early Permian. The Sibumasu Block collided with the Sukhothai Arc in the early Late Triassic, which formed the extensive accretionary prism of the Paleo-Tethys Suture Zone (CRL). The magmatism of the Sukhothai Arc ceased at the end of the Triassic [16, 25]. The Phayao Fault (PF), the Mae Chan Fault (MCF) and the Nam Ma Fault (NMF) are the three major faults in the Sukhothai

Block. The DBPF located in the east of the Sukhothai Block is an important left lateral strike slip fault in the Indochina region [26-27]. The average slip rate of the fault is 2.5 mm/y since the early Pliocene [28]. Six strong earthquakes (Ms≥5.0) occurred at the fault since 1900 which indicates the DBPF is an active fault.

3. Data and Methods

A total number of 73 heat flow data (Appendix, Table 1) is compiled from the Global Heat Flow Database of the International Heat Flow Commission [29] last updated in 2011 and the published papers [30-32]. The magnetic anomaly data used in this study is based on the Earth Magnetic Anomaly Grid [33-34], which is a 3 arc-minute resolution data set compiled from satellite, ship and airborne magnetic measurements. Comparison between the CPD estimated from the satellite magnetic data and the CPD estimated from the aeromagnetic data show that they are comparable [9, 35-36, 37].

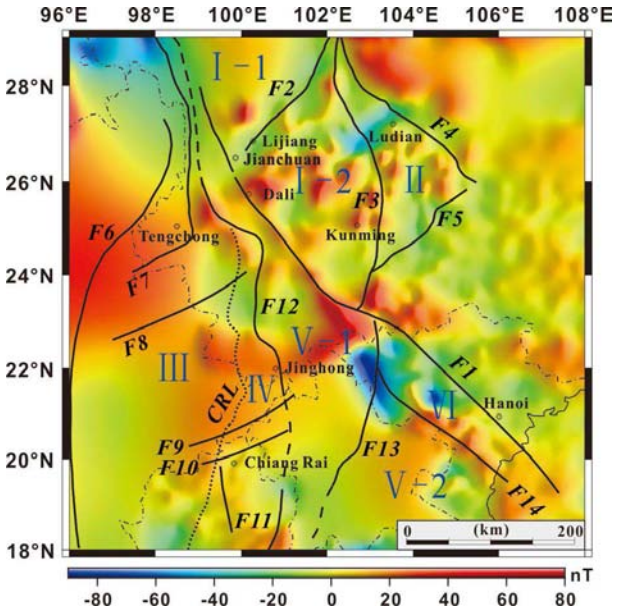

Figure 2. *The satellite magnetic anomaly at altitude 15 km after upwards continuation. The name of the faults and blocks in the Figure 2 are shown in Figure 1.*

The total intensity anomaly is 5 km above WGS84 ellipsoid. The measured magnetic anomaly consists of the anomalies generated by the shallow and deep magnetic bodies. The presence of the shallow magnetic bodies may reduce the accuracy of the data. Upward continuation of two-dimensional magnetic anomalies can effectively suppress the effect from the shallow bodies, thus highlighting the effect from the deep bodies [38]. The magnetic anomaly data used in this paper is 15 km above mean sea level after upward continuation for 10km, because the magnetic anomaly in this height effectively removes the anomalies generated by shallow magnetic bodies. The magnetic anomaly in the study area varies from -89 nT to 75 nT (Figure 2). Some researchers [39-41] confirmed that it is not necessary to reduce the spectrum to the pole (RTP). This is advantageous for calculating CPD at low magnetic latitudes where a RTP is difficult [39], because RTP is a phase operation which theoretically has no effects on estimated CPD, though there may exist a small spatial shift in CPD with RTP [42].

The method used in this paper to estimate the Curie surface depth is based on the spectral analysis method. Tanaka et al. [2] assumed that the layer extends infinitely far in all horizontal directions. The depth to the top bound of a magnetic source is small compared with the horizontal scale of a magnetic source, and that magnetization $M(x,y)$ is a random function of x and y. Blakely [41] introduced the power-density spectra of the total-field anomaly (P):

$$P_{\Delta T}(k_x,k_y) = P_M(k_x,k_y)\cdot F(k_x,k_y) \quad (1)$$

where $F(k_x,k_y) = 4\pi^2 C_m^2 |\Theta_m|^2 |\Theta_f|^2 e^{-2|k|Z_t}(1-e^{-|k|(Z_b-Z_t)})^2$, P_M is the power-density spectra of the magnetization, C_m is a proportionality constant, Θ_m and Θ_f are factors for magnetization direction and geomagnetic field direction. Besides, z_t and z_b are top and basal depth of magnetic source, respectively, k_x and k_y are the wavenumbers from the 2D Fourier expansion of the magnetic anomaly field in frequency domain, $k = \sqrt{k_x^2+k_y^2}$.

The above equation can be simplified by noting that all terms, except $|\Theta_m|^2$ and $|\Theta_f|^2$ are radially symmetric. Moreover, the radial average of Θ_m and Θ_f are constant. If $M(x,y)$ is completely random and uncorrelated, $\Phi_M(k_x,k_y)$ is a constant. Hence, the radial average of $P_{\Delta T}$ can be simplified as [7]:

$$\bar{P}_{\Delta T}(|k|) = Ae^{-2|k|Z_t}(1-e^{-|k|(Z_b-Z_t)})^2 \quad (2)$$

where A is a constant. By taking natural logarithm on both sides of eq. (2) it can get

$$\ln[\bar{P}_{\Delta T}(|k|)] = \ln A - 2|k|Z_t + 2\ln(1-e^{-|k|(Z_b-Z_t)}) \quad (3)$$

When wavelengths are smaller than twice of the thickness of the magnetized layers, eq.(3) approximately becomes

$$\ln[\bar{P}_{\Delta T}(|k|)^{1/2}] \approx \ln A - |k|Z_t \quad (4)$$

Thus, the depth of the top boundary Z_t can be estimated by fitting a straight line through the low wavenumbers of the power spectrum of $\ln[\bar{P}_{\Delta T}(|k|)^{1/2}]$ via eq. (4).

On the other hand, eq. (2) can be simplifies to

$$\bar{P}_{\Delta T}(|k|) = Ae^{-2|k|Z_0}(e^{-|k|(Z_t-Z_0)} - e^{-|k|(Z_b-Z_0)})^2 \quad (5)$$

where Z_0 is the depth to the central point of the magnetic source. At low wavenumber band, $e^{-|k|(Z_t-Z_0)} = e^{|k|(Z_b-Z_0)} \approx |k|(Z_b-Z_0)$, thus eq.(5) can be rewritten as

$$\bar{P}_{\Delta T}(|k|)^{1/2} \approx Be^{-|k|Z_0}(e^{|k|d} - e^{-|k|d}) = Be^{-|k|Z_0}\cdot(2|k|d) \quad (6)$$

where B is a constant and 2d is the thickness of the total magnetic source. Now by taking logarithms on both sides of eq. (6),

$$\ln[\bar{P}_{\Delta T}(|k|)^{\frac{1}{2}}/|k|] = \ln C - |k|Z_0 \quad (7)$$

where C is a constant.

Thus the central depth Z_0 is estimated by fitting a straight line through the high wavenumbers of the power spectrum of $\ln[\bar{P}_{\Delta T}(|k|)^{\frac{1}{2}}/|k|]$. Once Z_t and Z_0 are calculated, the depth to the bottom of the magnetic source can be derived [2, 40] as

$$Z_b = 2Z_0 - Z_t. \quad (8)$$

The obtained basal depth of the magnetic source is assumed to be the Curie point depth.

Previous studies show that the size of the optimal square window is about 4-6 times the estimated depth [43-44]. This paper divides the study area into a window of 150km×150km, and two neighboring windows have an overlapping of 50%. Then, $\ln[\bar{P}_{\Delta T}(|k|)^{1/2}]$ and $\ln[\bar{P}_{\Delta T}(|k|)^{\frac{1}{2}}/|k|]$ for each square using 2-D FFT power spectrum (Eqs. (4) and (7)) are calculated. The progress of estimating the Curie point depth of a window is shown in Figure 3. Finally, the CPD in the study area is calculated after interpolating.

The relationship between CPD (Z_b) and heat flow (q_s) can be described as [45]:

$$q_s = \lambda \frac{T_b - T_t}{Z_b - Z_t} + H_0 hr^2 \frac{e^{-Z_b/hr} - e^{-Z_t/hr}}{Z_b} + H_0 \cdot hr \cdot e^{-Z_t/hr} \quad (9)$$

where λ represents the coefficient of thermal conductivity, T_t, T_b is the temperature of the top and bottom of magnetic layer, H_0 is the heat production rate at the surface, hr is the characteristic drop off of H_0. It is assume that $T_b - T_t =$ 580K, Z_t=0, H_0=3.0×10^{-6}W/m^3, hr=10 km [46], then the theoretical curves of geothermal heat flow for different k are plotted.

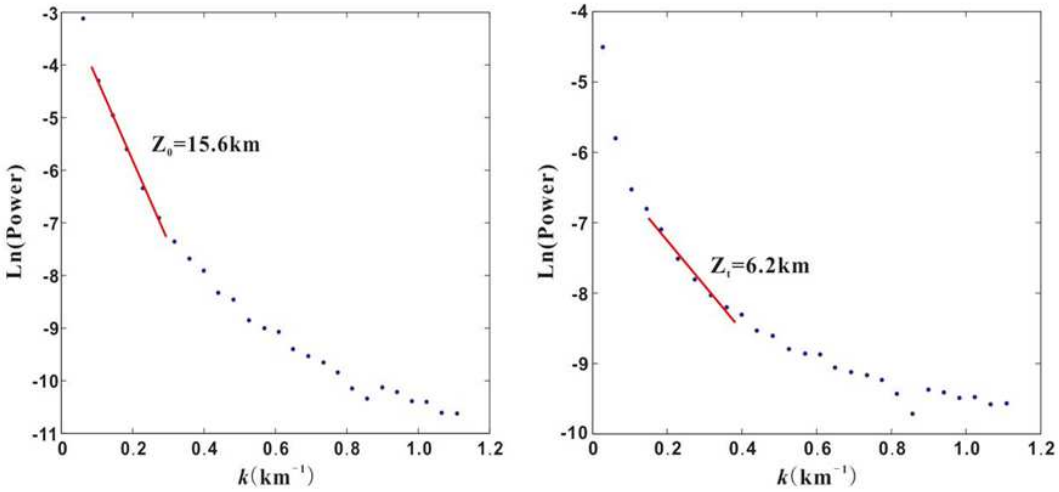

Figure 3. *The process of estimating the top depth Z_t and the central depth Z_0 of one window using power spectrum method. The absolute value of the slope of the red solid line represents Z_0 (Z_0 = 15.6 km) and Z_t (Z_t=6.2 km), respectively.*

4. Results

Results (Figure 4) show that the CPD ranges from 15 km to 36 km and the average depth is 26.33 km. The distributed characteristic of CPD on the north and south sides of the RRF are different. The CPD the south side is strip-like distribution, while the north side is cluster-like distribution. There are three parts with shallow CPD on the south side of the RRF (F1): the GLGF (F7) zone, the middle part of the Sukhothai Block (IV) and the DBPF (F13) zone, while two parts with deep CPD: the Lanping-Simao Block (V-1) and the middle part of the Sibumasu Block (III). On the north side of the RRF, CPD in the Eastern Yunnan Block (II), the middle XJF (F3) zone and the XJHF (F2) are shallow, while the northwest Sichuan Block (I-1), the central Yunnan Block (I-2) and the north and south part of the XJF are deep. In the study area, the shallowest CPD is 15.5 km, which is located in the Chiang Rai zone belongs to the middle of the Sukhothai block (IV). The average CPD is less than 20 km in this region. The deepest CPD is 35.2 km, which is located in the south part of the Northwest Sichuan Block zone where the average CPD is more than 30 km.

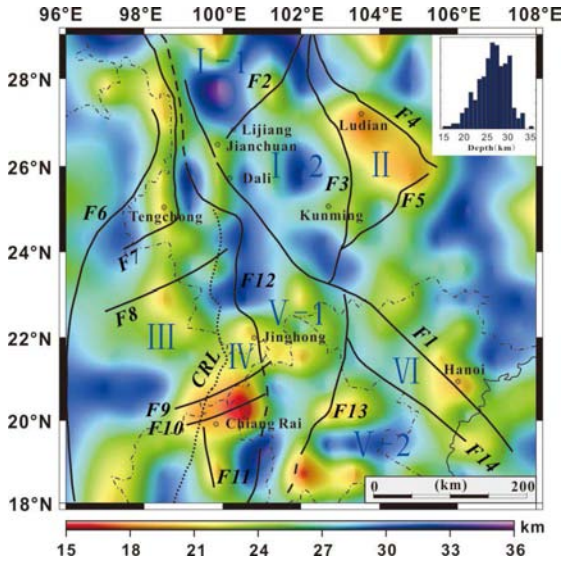

Figure 4. *Curie points depth map of the Southeast Tibet. In the upper right corner, the histogram shows the distribution range of the CPD in the study area. The abscissa indicates the depth of the CPD (at 1 km interval) and the ordinate indicates the number of Curie points. The name of the faults and blocks are shown in Figure 1.*

5. Discussion

5.1. CPD Versus Geological Structure

The Chuan-Dian rhombic block (CDRB, Figure 4, I) located in the north part to the RRF (Figure 4, *F*1) was divided by XJHF (*F*2) into the north part and the south part (I-1 and I-2). The fault cutting might induce the shallow CPD in the XJHF (*F*2) zone, while the north and south sides are deep. At the same time, as the eruption channel of the Emeishan basalt, the extension of the large deep fault which was caused by the Emeishan large igneous province in Late Paleozoic made the extensive eruption of the basalt along the fault [47], resulting in elevating the Curie point surface in this area. As the eastern boundary of the CDRB, the XJF (*F*3) plays an important role in the SE direction movement process of the block. The CPD in the central XJF zone is shallow. The average depth is about 23 km. However, the CPD in the northern and southern parts are more than 30 km. Previous tomography study in this area showed that the middle and lower crust beneath the XJF zone were characterized by low velocity anomaly, whereas the north and south crust are characterized by high velocity anomaly [48]. It is implied that the CPD distribution corresponds to the tomography velocity anomaly. There is a high velocity anomaly body in the southern XJF (F3) zone and it has a blocking effect on the southward movement of the CDRB. This phenomenon leads to strong deformations and strong earthquakes in the upper and middle crust. Therefore, the CPD of the southern XJF is deep, while strong earthquakes happen frequently.

The CPD distribution characteristics on the west and east sides of the XJF (F3) are different. The CPD in the Central Yunnan Block (I-2) is deep, whereas in the Eastern Yunnan Block (II) is especially shallow that is even shallower than 19 km. Tomographic results showed that a high velocity anomaly area beneath the Central Yunnan Block and a large low velocity anomaly area beneath the middle part of the Eastern Yunnan Block in the depth of 40 km [48]. Furthermore, the low velocity anomaly area decreased with the decrease of the depth and disappeared at 20 km depth. It is believed that the underplating process happened in the deep lower crust beneath the Eastern Yunnan Block might cause this phenomenon. The underplating process changes the geothermal field of deep crust, therefore, which leads to the increase of the temperature of the lower crust. It not only causes the generation of the large low velocity anomaly area, but also elevates the Curie point surface. Besides, it makes the CPD shallower in this region than that of the surrounding areas.

The Gaoligong CPD uplift zone in the Sibumasu Block (III) is characterized by GLGF (*F*7) and Nanting Fault (*F*8). The elevated CPD is caused by the underplating process. The process is that the Indian plate collided with the Eurasian plate, resulting in that the bottom of asthenosphere in this region partially upwelled since the Cenozoic period. The original basaltic magma originated from decompression melting induced underplating [49-50]. Seismic tomographic result shows that a low velocity anomaly area exists in the middle and lower of the crust in this region [51-52]. Previous studies in Tengchong zone showed that magma chambers in the crust were found [53-58]. The existence of the magma chambers changed the geothermal field, making the magnetic layer become thinner with the increased temperature. Consequently, the CPD is shallow.

The CPD in the Sukhothai Block (IV) presented strip-like shape. The shallowest CPD in the central part of Sukhothai Block is about 16 km. This block was characterized by PF (*F*11), MCF (*F*10) and NMF (*F*9). These faults were formed by the subduction between the Indian plate and the Eurasian plate [59]. The average left lateral slip rate of the MCF since the late Pleistocene was about 12 mm/y [60]. The average slip rate of the NMF was 0.6-2.4 mm/y [61]. Strong earthquakes above Ms.5 have occurred for several times around these faults [18, 62], indicating a strong tectonic movement in this region. The shallow CPD is probably caused by the strike slip movement of these faults. The frictional heat induced by the fault shearing movement induced the partial melting, and the anomalous heat sources within the crust formed [63]. The distribution of abundant hot springs in northern Thailand might possibly be related to these faults [59]. On the other hand, the formation of the Sukhothai Arc may have an effect on the geothermal field in the area. The volcanic arc system, Sukhothai Arc [10, 16, 64-67], was constructed in the late Carboniferous–early Permian on the margin of the Indochina Block (V) by northwards subduction of the Palaeo-Tethys. However, it is unlikely that the arc magmatism could influence the CPD distribution due to the age-old magmatism.

The DBPF CPD uplift zone is located in the DBPF (*F*13) zone. The regional crustal extension induced the upwelling of the deep mantle, making the basaltic magma in the DBPF zone quickly move to the surface in the Pliocene period [68]. The frictional heat induced by the fault and the upwelling of the deep mantle caused the shallow CPD in the DBPF zone.

5.2. CPD Versus Heat Flow

The heat flow is the energy that is transmitted from the interior of the earth to the surface in the unit area over the earth's surface per unit time and then distributed to the space of the universe. It can reflect the characteristics of a geothermal field [69]. A total number of 73 heat flow points are plotted on CPD distribution map (Figure 5). These measured heat flow points are mainly distributed in Yunnan, China and northern Thailand. The mean heat flow in study area is 70.48 mW/m^2, it is higher than the mean overall continental flow of China, 63 mW/m^2 [31]. Previous studies showed that the heat flow corresponds with the CPD [7, 36, 70-71]. The heat flow in the Central Yunnan Block (I-2) is low, while the CPD is deep. The heat flow in Tengchong is more than 118 mW/m^2 and the shallowest CPD is 21.7 km. The maximum heat flow in the northern Chiang Rai area reached 104 mW/m^2 and the CPD is shallower than perimeter, the shallowest point is only 20.4 km. However, heat flow in the Eastern Yunnan Block (II) is low with the average value 60 mW/m^2 [72], whereas the average CPD is as shallow as 20 km.

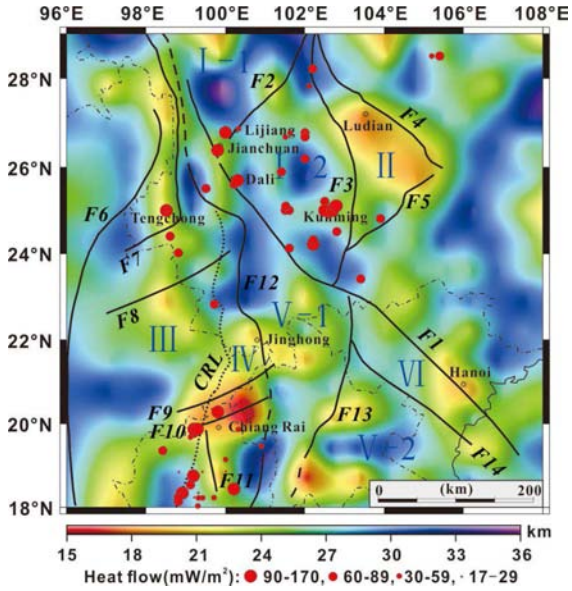

Figure 5. *The distribution of heat flow points at different values. The red dots of different sizes in the figure represent different values of the measured heat flow. The name of the faults and blocks are shown in Figure 1.*

Actually, measured heat flow is nonlinearly correlated with the calculated CPD [73]. Theoretical curves of heat flow for different thermal conductivities (λ) are plotted on Figure 6 based on Eq. (9). Most of the heat flow points are located between the theoretical curves of λ= 1 W (m°C) to λ= 5 W (m°C). This phenomenon indicates that the thermal conductivity varies greatly in different area in study area. According to Eq. (9), if λ changes 1W (m°C) in one heat flow point, the heat flow various ranges from 16.5 to 37.5 mW/m^2. It indicates that the heat flows are likely more influenced by thermal conductivity. Previous studies on the eastern and southeastern Asia, the north Atlantic and the South China Sea show that the low thermal conductivity of crustal rocks may induce a delay between the changed thermal field and the effect of heat flow [47, 73-74]. It is supposed that the low thermal conductivity might probably cause the low CPD with low heat flow in the Eastern Yunnan Block.

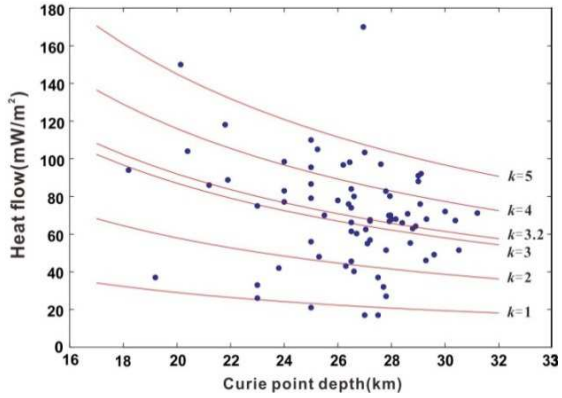

Figure 6. *Theoretical curves of heat flow. The blue points indicate the measured heat flow at different CPD in the study area, the red solid line represents the theoretical curves of the heat flow with different thermal conductivities, λ. λ=3.2 W / (m°C) is the thermal conductivity after fitting based on all the heat flows, it represents the average thermal conductivity of the magnetic layer throughout the study area.*

6. Conclusions

In the study area, the CPD ranges between 15 km and 36 km. The CPD distribution characteristics present cluster-like in the northern part and trip-like in the southern part, which are related to the geological and tectonic activities in the deep and shallow crust. The thermal disturbances caused by the tectonic activities in middle-lower crust, such as the subduction between the Eurasian plate and the Indian plate as well as the underplating beneath the Eastern Yunnan Block, could change the distribution of the underground geothermal field, resulting in influencing the distribution of the CPD. At the same time, the geological activities caused by the Xiaojinhe Fault, the Xiaojiang Fault, the Dien Bien Phu Fault, the Phayao Fault and the Mae Chan Fault also can result in shallow CPD. The thermal conductivities of the distinguishable zones in the study area are different. The low heat flow is probably related to the low thermal conductivity in the Eastern Yunnan Block.

Acknowledgements

The research was financially supported by National Natural Science Foundation of China (41606044) and Special Fund for Ocean Scientific Research in the Public Interest (201305029-02).

Appendix

Table 1. *Heat flow values and CPD of the 73 heat flow points.*

Longitude	Latitude	Heat flow value	CPD
99.2	18.8	170.0	26.9
99.3	19.9	150.0	20.1
98.5	25.0	118.1	21.8
100.2	18.5	110.0	25.0
102.8	25.1	105.0	25.2
99.2	19.9	104.0	20.4
100.3	25.7	103.4	27.0
99.8	26.4	98.5	24.0
111.2	22.6	98.2	26.4
100.0	26.8	97.1	27.6
102.5	25.0	96.7	26.2
102.7	25.0	95.5	25.0
99.8	20.3	94.0	18.2
102.2	24.2	92.1	29.1
98.9	18.4	91.0	29.0
98.5	25.0	88.8	21.9
98.8	18.2	88.0	29.0
102.7	25.0	86.6	25.0
99.2	19.8	86.0	21.2
102.0	26.8	84.0	26.5
98.4	19.4	83.0	24.0
101.6	25.0	82.8	27.8
101.5	25.1	80.2	27.9
102.5	25.2	80.0	26.6
102.7	25.0	79.1	25.0
102.6	24.9	77.9	26.0
98.8	24.0	77.1	24.0
102.2	24.3	76.0	29.1
100.2	25.6	76.0	26.4
98.6	24.4	75.0	23.0
110.2	18.7	74.0	26.5
102.0	26.2	72.0	30.0

Longitude	Latitude	Heat flow value	CPD
102.2	28.3	71.2	31.2
99.5	25.5	70.8	28.6
101.5	25.0	70.0	28.0
102.7	25.1	70.0	25.5
102.8	24.5	69.9	27.9
98.8	18.3	68.0	29.3
101.6	24.1	68.0	28.2
99.1	18.6	68.0	28.0
101.4	25.9	67.6	27.2
106.8	26.6	67.2	30.4
102.0	26.7	67.0	27.2
107.2	29.9	66.8	27.9
103.9	24.8	66.2	26.5
99.7	22.8	66.0	28.4
104.9	29.7	64.2	28.9
103.4	23.4	63.0	28.8
106.3	30.0	62.5	27.0
105.4	28.6	61.5	26.5
106.7	28.6	60.3	26.7
102.0	26.7	56.9	27.2
99.7	18.3	56.0	25.0
100.3	26.9	55.3	28.7
99.3	18.3	55.0	27.1
102.1	27.9	51.5	30.5
105.2	28.6	51.5	27.8
105.6	29.1	49.1	29.6
100.1	18.0	48.0	25.3
100.9	19.5	46.0	29.3
101.6	26.8	45.6	26.5
99.4	18.3	43.0	26.3
100.0	19.2	42.0	23.8
101.5	26.7	40.2	26.6
99.3	18.1	37.0	27.5
100.3	19.9	37.0	19.2
99.1	19.7	33.0	23.0
99.1	18.7	32.0	27.7
99.2	18.3	27.0	27.8
100.0	18.9	26.0	23.0
99.4	18.9	21.0	25.0
98.8	18.9	17.0	27.5
99.3	18.4	17.0	27.0

References

[1] Dunlop, D. J., Özdemir, Ö, 2001. Beyond Néel's theories: thermal demagnetization of narrow-band partial thermoremanent magnetizations. Physics of the Earth and Planetary Interiors, 126: 43-57.

[2] Tanaka, A., Okubo, Y., and Matsubayashi, O., 1999. Curie point depth based on spectrum analysis of the magnetic anomaly data in East and Southeast Asia. Tectonophysics, 306: 461-470.

[3] Dolmaz, M. N., Hisarli, Z. M., and Mer, T. U. 2005. Curie Point Depths Based on Spectrum Analysis of Aeromagnetic Data, West Anatolian Extensional Province, Turkey. Pure and Applied Geophysics, 162: 571-590.

[4] Aboud, E., Salem, A., and Mekkawi, M., 2011. Curie depth map for Sinai Peninsula, Egypt deduced from the analysis of magnetic data. Tectonophysics, 506: 46-54.

[5] Kasidi, S., Nur, A., 2012. Curie depth isotherm deduced from spectral analysis of Magnetic data over Sarti and environs of North-Eastern Nigeria. Sch J Biotech, 1: 49-56.

[6] Guimarães, S., Ravat, D., and Hamza, V., 2014. Combined use of the centroid and matched filtering spectral magnetic methods in determining thermomagnetic characteristics of the crust in the structural provinces of Central Brazil. Tectonophysics, 624: 87-99.

[7] Hsieh, H., Chen, C., Lin, P., and Yen, H. 2014. Curie point depth from spectral analysis of magnetic data in Taiwan. Journal of Asian Earth Sciences, 90: 26–33. doi: 10.1016/j.jseaes.2014.04.007.

[8] Shen, N., Li, C., Zhang, G., and Wang, H., 1986. Curie isotherm depths calculation from aeromagnetic anomalies over Xikang and Yunnan continental paleorift zone. Chinese Journal of Geophysics, 29 (5): 496–502.

[9] Gao, G., Kang, G., Bai, C., and Li, G., 2015. Study on crustal magnetic anomalies and Curie surface in Southeast Tibet. Journal of Asian Earth Sciences, 97: 169–177.

[10] Metcalfe, I., 2013. Gondwana dispersion and Asian accretion: tectonic and palaeogeographic evolution of eastern Tethys. Journal of Asian Earth Sciences, 66: 1-33.

[11] Xiang, H, F., Han, Z, J., Guo, S, M., Cheng, L, C., and Zhang, W., 2004. Processing about quantitative study of large-scale strike-slip movement on Red River Fault zone. Advance in Earth Science, 19(6): 56-59.

[12] Şengör, A, M, C., 1991. Plate tectonics and orogenic research after 25 years: A Tethyan perspective. Tectonophysics, 187: 315-344.

[13] Li, X, Z., Liu, Z, Q., Pan, and G, Y. 1991. Tectonic Units Division and Evolution History of Three -river Region in Southwest China. The Institute Journal of Chengdu Institute of Geology and Mineral Resources, Beijing : Geological Publishing House, 13: 1-150. [in Chinese.]

[14] Phan, C., Le, D., Le, D., 1991. Geology of Cambodia, Laos and Vietnam (Explanatory to the geological map Cambodia, Laos and Vietnam at 1:1000000 scale). Published by the Geological Survey of Vietnam.

[15] Lepvrier, C., Maluski, H., Van Tich, V., Leyreloup, A., Thi, P. T., and Van Vuong, N., 2004. The early Triassic Indosinian orogeny in Vietnam (Truong Son Belt and Kontum Massif); implications for the geodynamic evolution of Indochina. Tectonophysics, 393: 87-118.

[16] Sone, M., Metcalfe, I., 2008. Parallel Tethyan Sutures in mainland SE Asia: new insights for Palaeo-Tethys closure. Compte Rendus Geoscience, 340: 166–179.

[17] Tun, S. T., Wang, Y., Khaing, S. N., Thant, M., Htay, N., Htwe, Y. M. M., & Sieh, K., 2014. Surface ruptures of the Mw 6.8 March 2011 Tarlay earthquake, eastern Myanmar. Bulletin of the Seismological Society of America, 104(6), 2915-2932.

[18] Noisagool, S., Boonchaisuk, S., Pornsopin, P., and Siripunvaraporn, W., 2016. The regional moment tensor of the 5 May 2014 Chiang Rai earthquake (Mw= 6.5), Northern Thailand, with its aftershocks and its implication to the stress and the instability of the Phayao Fault Zone. Journal of Asian Earth Sciences, 127: 231-245.

[19] Roger, F., Calassou, S., Lancelot, J., Malavieille, J., Mattauer, M., Xu, Z., Hao, Z., and Hou, L., 1995. Miocene emplacement and deformation of the Konga Shan granite (Xianshui He fault zone, west Sichuan, China): Geodynamic implications. Earth & Planetary Science Letters, 201-216.

[20] Wang, E., Burchfiel, B. C., Royden, L. H., Chen, L., Chen, J., Li, W., and Chen, Z., 1998. Late Cenozoic Xianshuihe – Xiaojiang, Red River, and Dali Fault Systems of Southwestern Sichuan and Central Yunnan, China. Geological Society of America, 327: 108.

[21] Yokoyama, M., Liu, Y., Otofuji, Y. I., and Yang, Z., 1999. New Late Jurassic palaeomagnetic data from the northern Sichuan basin: implications for the deformation of the Yangtze craton. Geophysical Journal International, 139: 795–805.

[22] Chen, Z., Burchfiel, B., Liu, Y., King, R., Royden, L., Tang, W., Wang, E., Zhao, J., and Zhang, X., 2000. Global Positioning System measurements from eastern Tibet and their implications for India/Eurasia intercontinental deformation. Journal of Geophysical Research: Solid Earth, 105: 16215 – 16227.

[23] Lv, J.-N., Shen, Z.-K., Wang, M., 2003. Contemporary crustal deformation and active tectonic block model of the Sichuan-Yunnan region, China. Seismol. Geol, 25: 543-554. [in Chinese.]

[24] Qian, X, D, Qin J, Z., 2008. Strong Earthquake Risk Analysis of Xiaojiang Fault Zone and Surrounding Areas. Journal of Seismological Research, 31(4): 354-361. [in Chinese.]

[25] Metcalfe, I., 1996. Gondwanaland dispersion, Asian accretion and evolution of eastern Tethys∗. Australian Journal of Earth Sciences, 43: 605-623.

[26] Takemoto, K., Halim, N., Otofuji, Y. I., Tri, T. V., Le, V. D., and Hada, S., 2005. New paleomagnetic constraints on the extrusion of Indochina: Late Cretaceous results from the Song Da terrane, northern Vietnam. Earth & Planetary Science Letters, 229: 273-285.

[27] Tang, Y., Liu, J, L., Song, Z, J., 2009. Structural Characteristics of the Dien Bien Phu Strike Slip Fault Zone and its Regional Tectonic Implication. Acta Geologica Sinica, 83(10): 1401-1414. [in Chinese.]

[28] Lai, K.-Y., Chen, Y.-G., Lâm, D. Đ., 2012. Pliocene-to-present morphotectonics of the Dien Bien Phu fault in northwest Vietnam. Geomorphology, 173: 52-68.

[29] http://www.heatflow.und.edu/IHFC%20Database/Asia%20and%20Middle%20Eastern%20Countries/thailand.csv

[30] Wang J, Y., Huang, S, P., 1990. Compilation of heat flow data in the China continental area (2nd Edition). Seismilogy and Geology, 12(4): 351 —366. [in Chinese.]

[31] Hu, S., He, L, Wang, J., 2001. Compilation of heat flow data in the China continental area (4nd edition). Chinese Journal of Geophysics, 44(5): 611-626. [in Chinese.]

[32] Jiang, G. Z., Gao, P., and Rao, S. 2016. Compilation of heat flow data in the continental area of China (4th edition). Chinese Journal of Geophysics, 59(8): 2892-2910. [in Chinese.] doi: 10.6038/cjg20160815.

[33] Maus, S., Sazonova, T., Hemant, K., Fairhead, J., and Ravat, D., 2007. National geophysical data center candidate for the world digital magnetic anomaly map. Geochemistry Geophysics Geosystems, 80(6): Q06017.

[34] http://geomag.org/models/wdmam.html

[35] Rajaram, M., Anand, S. P., Hemant, K., and Purucker, M. E., 2009. Curie isotherm map of Indian subcontinent from satellite and aeromagnetic data. Earth & Planetary Science Letters, 281: 147–158.

[36] Gao, G., Kang, G., Bai, C., and Li, G., 2013. Distribution of the crustal magnetic anomaly and geological structure in Xinjiang, China. Journal of Asian Earth Sciences, 77: 12–20.

[37] Salazar, J. M., Vargas, C. A., and Leon, H., 2017. Curie point depth in the SW Caribbean using the radially averaged spectra of magnetic anomalies. Tectonophysics, 694: 400-413.

[38] Guan, Z., 2005. Geomagnetic field and magnetic exploration. Geological Publishing House, Beijing.

[39] Maus, S., Gordan, D., Fairhead, D., 1997. Curie-temperature depth estimation using a self-similar magnetization model. Geophysical Journal International, 129: 163–168.

[40] Okubo, Y., Graf, R., Hansen, R., Ogawa, K., and Tsu, H., 1985. Curie point depths of the island of Kyushu and surrounding areas, Japan. Geophysics, 50: 481-494.

[41] Blakely, R. J., 1995. Potential Theory in Gravity and Magnetic Applications. Cambridge University Press, Cambridge.

[42] Li, C, F., 2011. An integrated geodynamic model of the Nankai subduction zone and neighboring regions from geophysical inversion and modeling. Journal of Geodynamics, 51: 64–80.

[43] Dimitriadis, K., Tselentis, G.-A., and Thanassoulas, K., 1987. A BASIC program for 2-D spectral analysis of gravity data and source-depth estimation. Computers & Geosciences, 13: 549–560.

[44] Nwogbo, P., 1998. Spectral prediction of magnetic source depths from simple numerical models. Computers & Geosciences, 24: 847–852.

[45] Maule, C. F., Purucker, M. E., Olsen, N., and Mosegaard, K., 2005. Heat flux anomalies in Antarctica revealed by satellite magnetic data. Science, 309: 464-467.

[46] Jiao, L. G., 2014. Study seismicity by satellite lithospheric magnetic field and Curie isotherm depth inversion. Institute of Geophysics, China Earthquake Administration, Beijing.

[47] Li, H., Zhang, Z., Li, Y., and Wang, Y., 2013b. The location of the tail of Emeishan mantle plume. Geological Review, 59(2): 201–208. [in Chinese.]

[48] Wu, J, P, Yang, T., Wang, W, L. 2013. Three dimensional P-wave velocity structure around Xiaojiang fault system and its tectonic implication. Chinese Journal of Geophysics-Chinese Edition, 56(7): 2257-2267. [in Chinese.]

[49] Zhao D, Liu L., 2010. Deep structure and origin of active volcanoes in China. Geoscience Frontiers, 1(1): 31-44.

[50] Sun, Y., Wu, Z., Ye, P., Zhang, H., Li, H., and Tong, Y., 2016. Dynamics of the Tengchong volcanic region in the southeastern Tibetan plateau: A numerical study. Tectonophysics, 683: 272-285.

[51] Liu, F., Liu, J., Zhong, D., He, J., and You, Q., 2000. The subducted slab of Yangtze continental block beneath the Tethyian orogen in western Yunnan. Chinese Science Bulletin, 45: 466-472.

[52] Xu, Y., Yang, X., Li, Z., Liu, J., 2012. Seismic structure of the Tengchong volcanic area southwest China from local earthquake tomography. Journal of Volcanology & Geothermal Research, 239: 83-91.

[53] Bai, D., Meju, M. A., and Liao, Z., 2001. Magnetotelluric images of deep crustal structure of the Rehai geothermal field near Tengchong, southern China. Geophysical Journal International, 147: 677-687.

[54] Bai, D., Liao, Z., Zhao, G., and Wang, X., 1994. The inference of magmatic heat source beneath the Rehai (Hot Sea) field of Tengchong from the result of magnetotelluric sounding. Chinese Science Bulletin, 39(4): 344-347. [in Chinese.]

[55] Qin, J, Z., Huang, F, G., and Li, Q. 2000. 3-D chromatography of velocity structure in Tengchong volcano areas and nearby. Journal of Seismological Research, 23(2): 157-165. [in Chinese.]

[56] Huang, J., Zhao, D., and Zheng S., 2002. Lithospheric structure and its relationship to seismic and volcanic activity in southwest China. Journal of Geophysical Research: Solid Earth, 107(B10).

[57] Wang, C. Y., Chan, W. W., and Mooney, W. D., 2003. Three‐dimensional velocity structure of crust and upper mantle in southwestern China and its tectonic implications. Journal of Geophysical Research Solid Earth, 108(B9): 2442.

[58] Yang, H., Hu, J., Hu, Y., Duan, Y., and Li, G., 2013. Crustal structure in the Tengchong volcanic area and position of the magma chambers. Journal of Asian Earth Sciences, 73: 48-56.

[59] Amatyakul, P., Rung-Arunwan, T., and Siripunvaraporn, W., 2015 A pilot magnetotelluric survey for geothermal exploration in Mae Chan region, northern Thailand. Geothermics, 55: 31-38.

[60] Han X. M., Mao Y. P,, Zhang J. G., and Yang J. W., 2000. The geometric structure and the geomorphic sighs of Neo-activity in the Mae Chan Fault in North Thailand. Journal of Seismological Reasearch, 23(1): 67-71.

[61] Lacassin, R., Replumaz, A., and Leloup, P. H., 1998. Hairpin river loops and slip-sense inversion on southeast Asian strike-slip faults. Geology, 26: 703-706.

[62] Tun, S. T., Wang, Y., Khaing, S. N., Thant, M., Htay, N., Htwe, Y. M. M., Myint, T., and Sieh, K., 2014. Surface Ruptures of the Mw 6.8 March 2011 Tarlay Earthquake, Eastern Myanmar. Bulletin of the Seismological Society of America, 104(6): 2915-2932.

[63] Zhu, Y, Q., Shi, Y, L., 1990. Shear heating and partial melting of granite-thermal structure at overthrusted terrains in the greater Himalaya. Chinese Journal of Geophysics, 33(4): 408-416.

[64] Ueno, K., 1999. Gondwana/Tethys divide in East Asia: solution from Late Paleozoic foraminiferal paleobiogeography, Proceedings of the International Symposium on Shallow Tethys. Department of Geological Science: Chiang Mai University Chiang Mai, Thailand, pp. 45-54.

[65] Ueno, K., Hisada, K., 1999. Closure of the Paleo-Tethys caused by the collision of Indochina and Sibumasu. Chikyu Monthly, 21: 832–839. [in Japanese.]

[66] Ueno, K., Hisada, K. I., Ueno, K., and Hisada, K. I., 2001. The Nan-Uttaradit-Sa Kaeo Suture as a Main Paleo-Tethyan Suture in Thailand: Is it Real? Gondwana Research, 4: 804-806.

[67] Sone, M., Metcalfe, I., and Chaodumrong, P., 2012. The Chanthaburi terrane of southeastern Thailand: Stratigraphic confirmation as a disrupted segment of the Sukhothai Arc. Journal of Asian Earth Sciences, 61: 16-32.

[68] Koszowska, E., Wolska, A., Zuchiewicz, W., Cuong, N. Q., and Pécskay, Z., 2007. Crustal contamination of Late Neogene basalts in the Dien Bien Phu Basin, NW Vietnam: Some insights from petrological and geochronological studies. Journal of Asian Earth Sciences, 29: 1-17.

[69] Wang, J, Y, et al. 2015. Geothermics and its applications. Science Publishing House, Beijing.

[70] Lin, J, Y., Sibuet, J, C., and Hsu, S, K., 2005. Distribution of the East China Sea continental shelf basins and depths of magnetic sources. Earth Planets Space, 57: 1063—1072.

[71] Nuri, D, M., Ustaömer, T., and Hisarli, M, Z. 2005. Curie Point Depth variations to infer thermal structure of the crust at the African-Eurasian convergence zone, SW Turkey. Earth Planets Space, 57: 373—383

[72] Hu, S., He, L., and Wang, J., 2000. Heat flow in the continental area of China: a new data set. Earth and Planetary Science Letters, 179(2): 407-419.

[73] Li, C. F., Wang, J., 2016. Variations in Moho and Curie depths and heat flow in Eastern and Southeastern Asia. Marine Geophysical Research, 37: 1-20.

[74] Li, C, F., Shi, X., Zhou, Z., Li, J., Geng, J., and Chen, B., 2010. Depths to the magnetic layer bottom in the South China Sea area and their tectonic implications. Geophysical Journal International, 182: 1229-1247.